Magnetic Resonance Image-Based Modeling for Neurosurgical Interventions

Yongqiang Li[1,#], Changxin Lai[1,#], Chengchen Zhang[2], Alexa Singer[1], Suhao Qiu[1], Boming Sun[2], Michael S. Sacks[3] and Yuan Feng[1,*]

[1]Institute for Medical Imaging Technology, School of Biomedical Engineering, Shanghai Jiao Tong University, Shanghai, 200030, China.

[2]Department of Functional Neurosurgery, Rujin Hospital Affiliated to Shanghai Jiao Tong University School of Medicine, Shanghai, 200030, China.

[3]Department of Biomedical Engineering, University of Texas at Austin, Austin, Texas 78712, USA.

[#]Contributed equally. This paper is submitted for Y.C. Fung best paper award competition.

[*]Corresponding Author: Yuan Feng. Email: fengyuan@sjtu.edu.cn.

Abstract: Surgeries such as implantation of deep brain stimulation devices require accurate placement of devices within the brain. Because placement affects performance, image guidance and robotic assistance techniques have been widely adopted. These methods require accurate prediction of brain deformation during and following implantation. In this study, a magnetic resonance (MR) image-based finite element (FE) model was proposed by using a coupled Eulerian-Lagrangian method. Anatomical accuracy was achieved by mapping image voxels directly to the volumetric mesh space. The potential utility was demonstrated by evaluating the effect of different surgical approaches on the deformation of the corpus callosum (CC) region. The results showed that the maximum displacement of the corpus callosum increase with an increase of interventional angle with respect to the midline. The maximum displacement of the corpus callosum for different interventional locations was predicted, which is related to the brain curvature and the distance between the interventional area and corpus callosum (CC). The estimated displacement magnitude of the CC region followed those obtained from clinical observations. The proposed method provided an automatic pipeline for generating realistic computational models for interventional surgery. Results also demonstrated the potential of constructing patient-specific models for image-guided, robotic neurological surgery.

Keywords: Brain biomechanics; finite element model; intervention; magnetic resonance image (MRI)

1 Introduction

Image-guided surgery can achieve optimal performance with accurate target location in the brain. It can also be integrated with various robotic manipulation systems for remote surgery and delicate operations [1]. Among all forms of surgical procedures, image-guided brain intervention is a common practice for deep brain stimulation (DBS). However, deformation of brain tissue could occur during the interventional process due to its soft and viscoelastic properties. The deformed brain tissue poses a challenge for the current image guidance, which requires registration between the pre-operative and intra-operative images [2]. Therefore, quantification of the brain tissue deformation during the intervention is significant for accurate image guidance.

Intraoperative magnetic resonance (MR) imaging techniques can provide accurate information for image guidance in neurological surgery. Studies on MR imaging techniques for brain intervention can provide quantitative information for both image guidance and device manipulation by considering the brain tissue deformation [3,4]. For different modeling methods of predicting the brain deformation, finite element (FE) method could provide the most accurate estimation [5,6]. In addition, computational results of the FE

model can also provide information for force feedback, which is crucial for robotic manipulations.

Most of the current FE models of the brain are based on general anatomical structures, which lack geometrical details of the brain [7]. Although the general brain models could provide important information for quantifying the brain responses during the interventional process, patient-specific models are still needed for clinical applications. In DBS, electrodes, inserted into the brain in specific positions, required accuracy of sub-millimeter. Therefore, with available pre- and intra-operative MR images, a new FE model used for surgery is still needed.

In this study, the estimated displacement magnitude of the corpus callosum (CC) region was evaluated by finite element (FE) simulation of an interventional needle inserted into a brain. In Section 2, an MR-image based finite element (FE) modeling of the brain was proposed with anatomical details. The brain tissues were treated as hyperelastic, viscoelastic materials. The coupled Eulerian-Largrangian (CEL) method was adopted for the fluid environment of the brain tissue. The effects of interventional angles and locations for optimal surgery were studied in Section 3. In Section 4, the interventional results were presented and discussed. Preliminary results provided the suggestions of the optimal interventional course for minimal deformation of the brain tissue.

2 Methods

2.1 Mesh Generation and Simulation Configuration

The image-based human brain model was generated based on the reconstruction of MR atlas images from UCLA Brain Mapping Center [8]. By considering the biomechanical fidelity, the anatomical regions of white matter (WM), gray matter (GM), brain stem (BS), cerebellum (CB), cerebro-spinal-fluid (CSF), corpus callosum (CC), and blood vessel (VE) were segmented from brain MR images and constructed in the model. Briefly, each voxel from the MR image was extracted and mapped into a physical coordinate system. Then the connections of each node were established to build the mesh. The 2 mm isotropic hexahedron meshes for different brain regions were generated in this study. The details of the brain model generation process are shown in Fig. 1.

For the interventional FE model construction, a rigid interventional needle was constructed and inserted aligned with midline position perpendicular to the brain transverse plane. Both the brain and needle were placed in a fluid environment by using the Eulerian domain, which is shown in Fig. 2(a). For the FE simulation, the total intervention depth was 10 mm simulated with an increment of 1 mm, the brain stem was fixed as a boundary condition, which is shown in Fig. 2(b). In order to study the interaction between the interventional needle and surrounding CSF of brain, the coupled Eulerian-Largrangian (CEL) analysis method was introduced. For the CEL method, the complex material distributions in an Eulerian element mesh was assigned with the help of volume fraction tool in Abaqus/CAE. All simulations in the current study were conducted with ABAQUS/Explict 6.17 (Simulia, Providence, RI).

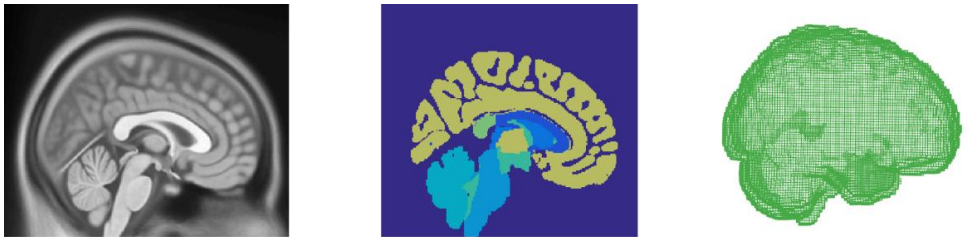

Figure 1: Construction of an image-based brain model. (a) A sample structural MR image of a brain. (b) Segmented brain regions in a sagittal plane including WM, GM, BS, BE, CSF, CC and VE. (c) A constructed FE brain model

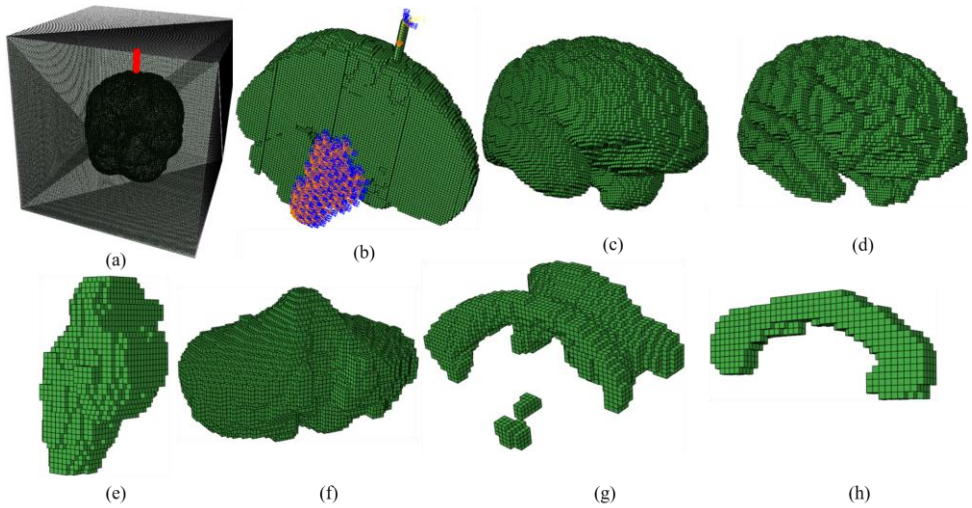

Figure 2: (a) The CEL model constructed with the box containing the computational domain. (b) The sagittal sectional interventional model with initial condition and boundary conditions. The brain model contains (c) WM, (d) GM, (e) BS, (f) CB, (g) CSF, and (h) CC

2.2 Model Computation

Considering large deformation of and rate effect of the brain tissue, a hyper-viscoelastic material model was employed [9-11]. In current study, a second-order Ogden model was employed to describe the hyperelastic behavior of brain tissue [12]

$$W = \sum_{i=1}^{N} \frac{\mu_i}{\alpha_i}\left(\lambda_1^{\alpha_i} + \lambda_2^{\alpha_i} + \lambda_3^{\alpha_i}\right) + \frac{K}{2}(J-1)^2, \quad (1)$$

where μ_i and α_i are the material constants, K is the bulk modulus, λ_i are the three principal stretches and the Jacobian $J = det\mathbf{F} = \lambda_1\lambda_2\lambda_3$. The total second Piola-Kirchhoff stress in the brain can be obtained as [13]

$$S_{ij} = S_{ij}^{e} + S_{ij}^{v}, \quad (2)$$

where S_{ij}^{e} is the hyperelastic part of the second Piola-Kirchhoff stress, it can be calculated directly from Eq. (1). The viscous part of the second Piola-Kirchhoff stress S_{ij}^{v} can be described as [14]

$$S_{ij}^{v} = \int_0^t G_{ijkl}(t-\tau)\frac{\partial E_{kl}}{\partial \tau}d\tau, \quad (3)$$

where E_{kl} are the components of the Green-Lagrangian strain tensor, G_{ijkl} are the stress relaxation functions, and t is the current time. The general form of G_{ijkl} can be further written as [13,14]

$$\mathrm{G}_{ijkl} = \frac{1}{3}[g_2(t) - g_1(t)]\delta_{ij}\delta_{kl} + \frac{1}{2}g_1(t)(\delta_{ik}\delta_{jl+}\delta_{il}\delta_{jk}), \quad (4)$$

where g_1(t) and g_2(t) are two independent relaxation functions. Each of the relaxation functions can be described using a Prony series equation [15]

$$g_R(t) = \frac{G_R(t)}{G_0} = 1 - \sum_{i=1}^{N} g_i(1 - e^{-t/\tau_i}), \quad (5)$$

where G_0 is the instantaneous shear relaxation modulus, N is the number of term, g_i is the relaxation modulus, and τ_i is the relaxation time. The material parameters are given in Tab. 1 and Tab. 2.

Table 1: Parameters of the Ogden model for brain tissue [9]

Region	Density (kg/m^3)	μ_1 (kPa)	μ_2 (kPa)	α_1	α_2	D_1
Gray matter	1040	77.27	12.47	5.67	4.56	9.13e-10
White matter	1040	35.98	46.9	1.15	0.199	9.13e-10

Table 2: Viscoelastic properties for brain tissue [9]

Region	g_1	g_2	g_3	$\tau_1(s)$	$\tau_2(s)$	$\tau_3(s)$
Grey matter	0.00078	0.1606	0.8261	11.05	0.0088	4.43e-4
White matter	0.0087	0.001	0.965	7.38	0.0572	2.52e-4

In current study, CSF was described as hyperplastic material using Neo-Hookean model, the material parameters are given in Tab. 3.

Table 3: Material constants for CSF [9]

Material	Density (kg/m^3)	C_{10} (kPa)	D_1
CSF	1040	11.27	9.13e-10

For the fluid environment domain material, it can be described by the linear *Us-Up* Hugoniot form of the Mie-Gruneisen equation of state (EOS), which is written as

$$p = \frac{\rho_0 c_0^2 \eta}{(1-s\eta)^2}\left(1 - \frac{\Gamma_0 \eta}{2}\right) + \Gamma_0 \rho_0 E_m, \tag{6}$$

where p is the current pressure, ρ_0 is the initial density, η is the nominal volumetric strain, c_0, s and Γ_0 are materials constants, and E_m is the internal energy per unit mass of the fluid. c_0 and s have the following relation

$$U_s = c_0 + sU_p, \tag{7}$$

where $\mathbf{U_s}$ is the shock velocity and U_p is the particle velocity (Tab. 4). The interventional needle is treated as a rigid body in the model (Tab. 5).

Table 4: Material constants for Water [16]

Material	Density (kg/m^3)	*Viscosity* (Ns/m^2)	c_0 (m/s)	s	Γ_0
Water	1000	1e-2	1480	0	0

Table 5: Material property of intervention needle

Material	Density (kg/m^3)	E (GPa)	v
Steel projectile	7800	210	0.3

3 Results

3.1 Effect of Interventional Angles for Optimal Surgery

Interventional angles ranging from 0 to 45 degrees with an increment of 10 degrees were simulated (Figure 3). As a demonstration, displacement distribution of the CC region was compared. It is seen from Fig. 3 that the maximum displacement values in CC increase with an increase of interventional angles with respect to the midline.

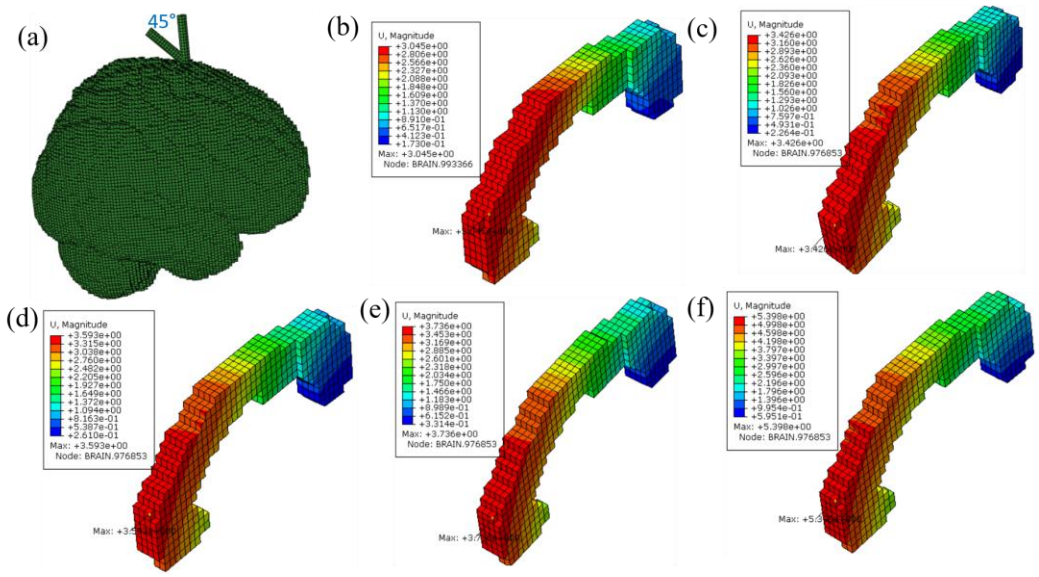

Figure 3: Displacement distributions of CC for interventional angles ranging from 0 to 45 degree. (a) Interventional position and angle range. Distribution of displacement magnitude for (b) 0, (c) 10, (d) 20, (e) 30, and (f) 45 degrees

3.2 Effect of Interventional Locations for Optimal Surgery

The brain deformation under different interventional locations was investigated by varying the interventional positions on top of brain with an incline angle of 30 degrees (Figure 4). It is seen from Fig. 4 that interventional location close to the midline (P1) had the largest magnitude of displacement for the CC region, followed by locations of P2, P7, P5, P4, and P3. The smallest deformation of CC was from the interventional location at P6.

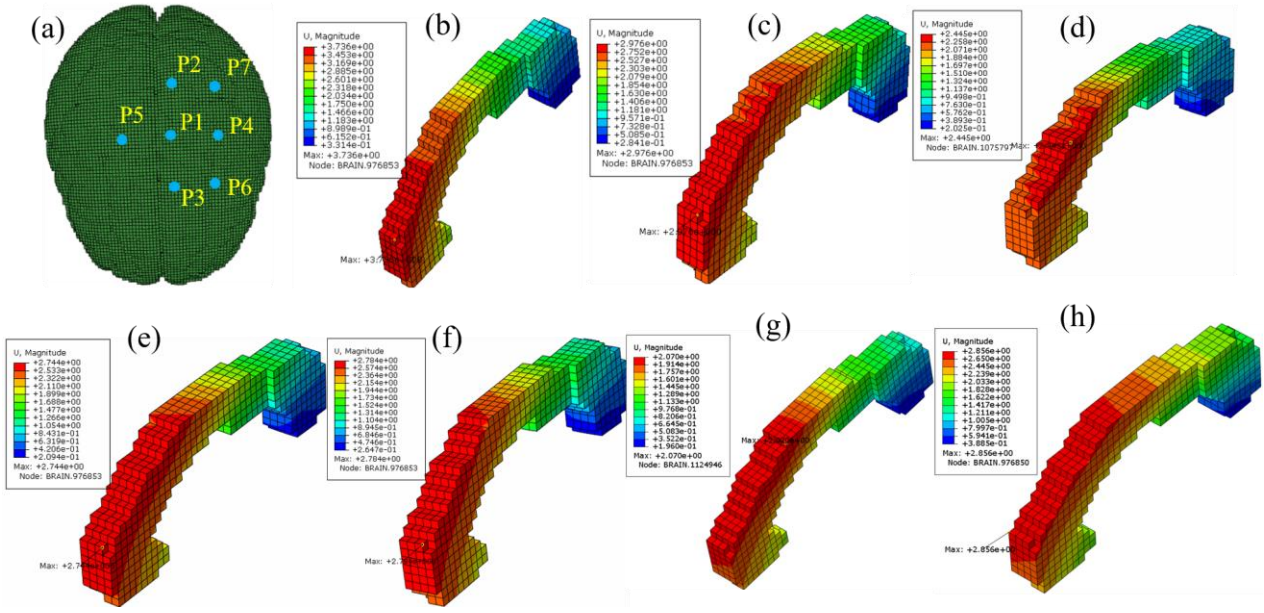

Figure 4: Distribution of the displacement magnitude of CC from interventions at (a) the 7 different locations on top of the brain. (b-h) intervention positions at locations P1 to P7

4 Discussion and Conclusions

Brain deformation during the interventional process affects the accuracy and performance of the surgery. To accurately quantify the deformation of the brain during the intervention, a model construction scheme based on MR images was proposed. Intervention process was simulated based on the FE model generated from the MR images. By varying the angles and locations of the intervention, deformation of the CC region was quantified and analyzed.

For varying angle of the intervention, simulation results showed that the largest deformation of CC resulted from the insert angle of 45 degrees direction parallel to the midline. This indicates that the smaller insert angle will have smaller displacement of corpus callosum during the interventional process. For varying intervention positions, simulation results from the CC region showed a decreasing order of the displacement for locations of P1, P2, and P3, which should be related to both the decreased inclined angles with the curvature effect and the shorter distance between insert needle and corpus callosum of P2 and P3. Similarly, locations P7, P4, and P6 has decrease trends due to the brain curvature effect. Location P4 and P5 have similar displacement of corpus callosum due to the symmetry of the brain. According to the simulation results, location P6 has the smallest displacement value of corpus callosum, which may be the optimal location for interventional surgery.

In this paper, a workflow to construct brain interventional FE model based on MR images was proposed. Within this framework, patient-specific models could be constructed for specific surgical applications. For illustration, the deformation of the corpus callosum is investigated. Using CEL modeling, brain deformation was quantified with improved computational accuracy. Results showed that the maximum displacement of CC region increased with an increase of interventional angles with respect to the midline. However, the maximum displacement of CC for different interventional locations depended on the brain curvature and interventional depth. This study demonstrated the potential of using MR image-based modeling for optimal interventional planning of image-guided, robotic neurological surgery.

Acknowledgement: Grant 31870941 from NSFC, grant 1944190700 from Shanghai Science and Technology Committee (STCSM).

References

1. Carter TJ, Sermesant M, Cash DM, Barratt DC, Tanner C et al. Application of soft tissue modelling to image-guided surgery. *Medical Engineering & Physics* **2005**, 27(10): 893-909.
2. Miga MI. Computational modeling for enhancing soft tissue image guided surgery: an application in neurosurgery. *Annals of Biomedical Engineering* **2016**, 44(1): 128-138.
3. Morin F, Courtecuisse H, Reinertsen I, Le Lann F, Palombi O et al. Brain-shift compensation using intraoperative ultrasound and constraint-based biomechanical simulation. *Medical Image Analysis* **2017**, 40: 133-153.
4. Iversen DH, Wein W, Lindseth F, Unsgård G, Reinertsen I. Automatic intraoperative correction of brain shift for accurate neuronavigation. *World Neurosurgery* **2018**: 1071-1078.
5. Ji S, Liu F, Roberts D, Hartov A, Paulsen K. Brain-skull boundary conditions in a neurosurgery deformation model. *Proceedings of Medical Imaging 2007: Visualization and Image-Guided Procedures* **2007**, 6509.
6. Ji S, Roberts DW, Hartov A, Paulsen KD. Brain-skull contact boundary conditions in an inverse computational deformation model. *Medical Image Analysis* **2009**, 13(4): 659-672.
7. Tonutti M, Gras G, Yang GZ. A machine learning approach for real-time modelling of tissue deformation in image-guided neurosurgery. *Artificial Intelligence in Medicine* **2017**, 80: 39-47.
8. Mazziotta JC, Toga AW, Evans A, Fox P, Lancaster J. A probabilistic atlas of the human brain: theory and rationale for its development: the international consortium for brain mapping (ICBM). *NeuroImage* **1995**, 2: 89-101.
9. Cotton RT, Pearce CW, Young PG, Kota N, Leung AC et al. Development of a geometrically accurate and adaptable finite element head model for impact simulation: the naval research laboratory-simpleware head model. *Computer Methods in Biomechanics and Biomedical Engineering* **2016**, 19(1): 101-113.

10. Finan JD, Sundaresh SN, Elkin BS, McKhann II GM, Morrison III B. Regional mechanical properties of human brain tissue for computational models of traumatic brain injury. *Acta Biomaterialia* **2017**, 55: 333-339.
11. Kleiven S. Predictors for traumatic brain injuries evaluated through accident reconstructions. https://doi.org/10.4271/2007-22-0003. **2007**.
12. Ogden RW. Non-Linear Elastic Deformations. Chichester, England: Ellis Harwood Ltd. **1984**.
13. Li YQ, Gao XL. Modeling of head injuries induced by golf ball impacts. *Mechanics of Advanced Materials and Structures*. https://doi.org/10.1080/15376494.2018.1446570. **2018**.
14. Christensen RM. Theory of Viscoelasticity: An Introduction, 2nd Edition. New York: Academic Press. **1982**.
15. Chafi MS, Karami G, Ziejewski M. Biomechanical assessment of brain dynamic responses due to blast pressure waves. *Annals of Biomedical Engineering* **2010**, 38(2): 490-504.
16. Akula P, Hua Y, Gu L. Blast-induced mild traumatic brain injury through ear canal: a finite element study. *Biomedical Engineering Letters* **2015**, 5(4): 281-288.